Solar Energy Materials & Solar Cells 246 (2022) 111917

Contents lists available at ScienceDirect

Solar Energy Materials and Solar Cells

journal homepage: www.elsevier.com/locate/solmat

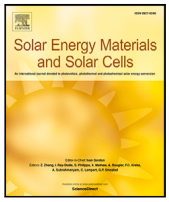

Photovoltaic photographs

Jeroen Hustings [a], Nico Fransaert [a], Kristof Vrancken [b], Rob Cornelissen [a], Roland Valcke [c], Jean V. Manca [a,*]

[a] UHasselt, X-LAB, Agoralaan D, Diepenbeek, 3590, Limburg, Belgium
[b] LUCA, School of Arts, C-Mine 5, Genk, 3600, Limburg, Belgium
[c] UHasselt, Molecular and Physical Plant Physiology, Agoralaan D, Diepenbeek, 3590, Limburg, Belgium

ARTICLE INFO

Keywords:
Patterned solar cells
Dye-sensitized solar cells
Building-integrated photovoltaics
Photographic process

ABSTRACT

In the field of photovoltaics (PV), an important trend is to increase the aesthetic and creative design aspects of solar cells towards more attractive and customized devices for integration in for instance architecture, *e.g.* building integrated photovoltaics (BIPV). Here we introduce the concept of "photovoltaic photographs", defined as semi-transparent solar cells (STSC) that are treated with a light-induced process to integrate an image in the photoactive layer, allowing creative applications such as photovoltaic photographs, paintings, posters, etc. Contrary to previously reported patterning processes used in emerging photovoltaics such as inkjet printing or methods where patterned transparent foils are assembled on top of the solar cells, the approach proposed here to obtain a patterned 2D-photoactive layer, is by using a direct photo-induced patterning process based on photobleaching of chromophores. Proof-of-principle demonstrators have been realized using dye-sensitized solar cells and the obtained insights can open the way to the exploration of combining this concept with other PV technologies.

1. Introduction

In the field of photovoltaics (PV), an important trend is to increase the aesthetic and creative design aspects of solar cells towards more attractive and customized devices for integration in for instance architecture (*e.g.* building integrated photovoltaics BIPV) and cars (*i.e.* automobile integrated photovoltaics AIPV) [1]. Recent evolutions in this domain are situated in all classes of PV, from conventional silicon technology to emerging PV such as organic solar cells (OPV), dye-sensitized solar cells (DSSC) and perovskite solar cells (PSC). The latter technologies provide additional degrees of design freedom, as they can be processed by wet deposition techniques and allow the realization of semi-transparent solar cells (STSC) and the use of various colors. In the following paragraphs, a brief overview is provided of the current state-of-the-art in relation to colored and patterned solar cells.

In STSCs, patterns correspond to a controlled spatial variation of device transparency and color, both of which are primarily related to compositional and structural properties of the active layer and the electrodes. Since photovoltaic power generation requires the absorption of light, STSCs are burdened with an intrinsic trade-off between efficiency and transparency.

General strategies to build STSCs include the use of ultrathin active layers – which is applicable to both hydrogenated amorphous Si (a-Si:H) solar cells [2] and emerging technologies such as OPVs, PSCs and DSSCs [3,4] – and the use of active materials with low absorption in the visible range [5,6]. Alternatively, transparency can be achieved by creating gaps between the active material, *e.g.* by laser scribing patterns [7], mesh-assisted self-assembly [8], or by replacement of uniform films by micro-holes [2] or "islands" of active material—as has been demonstrated with neutral-color semi-transparent perovskite solar cells [9]. Color-tuning often involves the use of colored electrodes [7,10] or the introduction of additional reflecting layers such as one-dimensional photonic crystals and light coupling layers [3,10]. Of course, the chemical composition of the active material influences the color of OPVs and PSCs [2,10–12], and "color-tinting" has been realized by adding a dye to the hole transporting medium of initially neutral-colored PSCs [9]. In DSSCs, the light absorbing dye is the vital component regarding color [13] – and optical properties can be tuned with quantum dot size in so-called quantum-dot-sensitized solar cells [14,15] – but the color and transparency of the electrolyte also influences the appearance of the final device [16].

Much research has been dedicated to the development of top electrodes that are both highly conductive and semi-transparent. Conventional metal film top electrodes are usually reflective, but trans-

* Corresponding author.
E-mail address: jean.manca@uhasselt.be (J.V. Manca).

https://doi.org/10.1016/j.solmat.2022.111917
Received 3 May 2022; Received in revised form 15 July 2022; Accepted 18 July 2022
Available online 29 July 2022
0927-0248/© 2022 The Authors. Published by Elsevier B.V. This is an open access article under the CC BY-NC-ND license (http://creativecommons.org/licenses/by-nc-nd/4.0/).

parency can be achieved by making the films ultrathin [17,18]—however, the trade-off in conductivity is generally considered non-profitable [10]. Therefore, conventional metal films are routinely replaced by silver nanowires in OPVs and PSCs, except in DSSCs where the liquid electrolyte causes poor stability of the nanowires [3,10]. Non-metal high performance transparent electrodes have been developed – ranging from transparent conductive oxides [19,20] to conducting polymers [21,22] and carbon materials [23–26] – with a focus on stability and processability [2,10]. When considering aesthetic and BIPV applications, additional aspects such as color-neutrality become important.

One way to achieve colored solar cells is by the application of color coatings. This method is used on black solar cells, *e.g.* a-Si, to raise their aesthetic value [27]. Besides covering PVs with semi-transparent foils or printing a pixelated pattern on the outer glass [28], the most straightforward way of displaying patterns with PVs is by connecting conventional solar cells in an arrangement, which is exemplified by the mosaic module concept based on metal-wrap-though cells [29]; however, with this approach, the sub-cells are opaque and their size limits the resolution. More flexible single-cell patterning methods are searched for in the fields of semi-transparent dye-sensitized, organic and perovskite solar cells. A recent study regarding DSSC anodes stained by inkjet printing demonstrated multi-colored solar cells with tailored transparency [30], and monochrome logos and images have been inkjet-printed using perovskite precursor ink [31]. Moreover, precise removal of materials by computer-controlled non-thermal laser ablation allowed for manipulation of transparency and aesthetic pattern design in PSCs [32].

Although research on DSSCs has grown significantly over the last two decades, performance – lab record efficiency of 12.25% [33] – and stability restrictions are at present the main obstacles to compete with conventional silicon solar cells, which dominate the PV market [34,35]. However, DSSCs offer differentiating intrinsic properties, which could lead to creative niche applications beyond the reach of silicon solar cells. As with OPVs and PSCs [36,37], DSSCs can be fabricated into flexible, semi-transparent modules available in wide color ranges at low production costs [34,38], which are appealing features for aesthetic purposes. The colored sensitizers used in DSSCs are mainly synthetic dyes, usually transition metal complex based compounds or organic dyes [39,40]. Alternatives are natural dyes (*e.g.* chlorophylls, anthocyanins, carotenoids,..) whose popularity originates from their relative abundance, large absorption in the visible spectrum, ease of preparation, cost effectiveness and eco-friendliness [40,41], but in general suffer from low efficiency and stability issues compared to their synthetic substitutes.

The semi-transparent character and ease of color implementation place DSSCs on the forefront of BIPV and AIPV [1]. One such example is the development of smart windows in zero energy buildings [38,42], with large-scale installations having been introduced over a decade ago [43] and successful long-term outdoor testing supporting the concept [44]. Recent works discussing the use of semi-transparent DSSCs as PV windows are reviewed elsewhere [45,46]. These PV glass modules do not only produce electricity, but also provide a wide variety of solar shading, which is made possible through the color tuning ability of these devices [47]. BIPVs also affect the image of our cities by providing buildings with an attractive and environmentally-friendly appearance. Specifically, when applied in large quantities, they contribute to the reduction of carbon emissions, while at the same time servicing an aesthetic or shading purpose.

It is clear that significant progress has been made in the realization of uniform colored photovoltaic films, with however only limited attention to patterned devices, *e.g.* through inkjet-printing or add-on transparent printed patterns. In the evolution towards more aesthetical solar cells, here the proposed innovation consists of integrating an image (photographs, paintings, geometric and graphical patterns, text,..) with photo-active functionality into the STSC using a direct photo-induced patterning process. Key advantages of this approach include: (1) preparation time is independent of size, (2) patterning process is compatible with the traditional production process, (3) no external, fragile foil is needed, (4) high-resolution patterning is possible, and (5) this methodology could possibly be applied to various classes of solar cells, specifically technology based on photosensitive absorbing layers that are prone to bleaching (*e.g.* OPV and PSC [48–50]).

As a proof-of-principle for the concept of photovoltaic photographs, demonstrators (up to 9×9 cm^2) have been realized using DSSCs, due to ease of fabrication and broad variety of available colors. In the following sections the photo-induced patterning process and the preparation and results of photovoltaic photographs will be presented. The ultimate goal of this endeavor is the introduction of photovoltaic photographs as a potential novel route to enhance the aesthetical and design possibilities for a variety of PV technologies.

2. Materials and methods

2.1. Direct photo-induced patterning of 2D-photoactive layer

The approach proposed here to obtain a patterned 2D-photoactive layer is by using a direct photo-induced patterning process, *i.e.* one-step photolithography in the presence of oxygen to induce selective photobleaching in the photoactive layer of organic-based solar cells. The method differs from traditional photolithography as employed in for instance semiconductor industry, as here no sacrificial resist film is needed, and no additional etching steps or chemical removal steps are required.

The approach to pattern the photoactive layer of organic-based solar cells to realize photovoltaic photographs is inspired by the anthotype photographic process; an ancient photographic method of transferring images from a transparency film to a sheet of paper (see Fig. 1). This invention can be attributed to Sir John Herschel (1792–1871) [51,52]. An anthotype photograph starts out as a sheet of paper dyed with a pigment extracted from mostly natural sources, such as berries, leaves, petals, ...A mask containing the desired image is placed over the dyed sheet, whereafter the assembly is left exposed to sunlight. This process will cause the underlying sheet to bleach in areas that are exposed to the light, while covered areas remain dark. The result is a monochromatic photograph of the image from the mask. Depending on the type of dye, the anthotype process can take from a couple of hours to a few days to develop. Recently, the anthotype technique has been rediscovered in several domains; for instance, for producing motifs on textile [53] and in the artistic work of experimental photographers such as co-author K. Vrancken [54].

2.2. Preparation of proof-of-principle photovoltaic photographs using DSSCs

The proposed procedure towards DSSC-based photovoltaic photographs using light-induced processes consists of the following general steps: first, the TiO_2 anode is dyed with a synthetic or natural dye. A transparent sheet (mask) containing the desired image is placed over the dyed electrode, and the assembly is exposed to a light source (see Fig. 2). The result is a monochromatic photograph that looks like the original image. For this process, the underlying photoanode will bleach in areas that are exposed to light, while covered areas remain dark.

By following this procedure we realized several proof-of-principle photovoltaic photographs based on different colors, offering a renewable energy source while servicing an aesthetic purpose. A detailed description of the fabrication process is discussed in the following paragraphs.

2.3. Materials

Experiments were done using two different types and sizes of anode material. Both types of DSSCs were built using pre-sintered titania

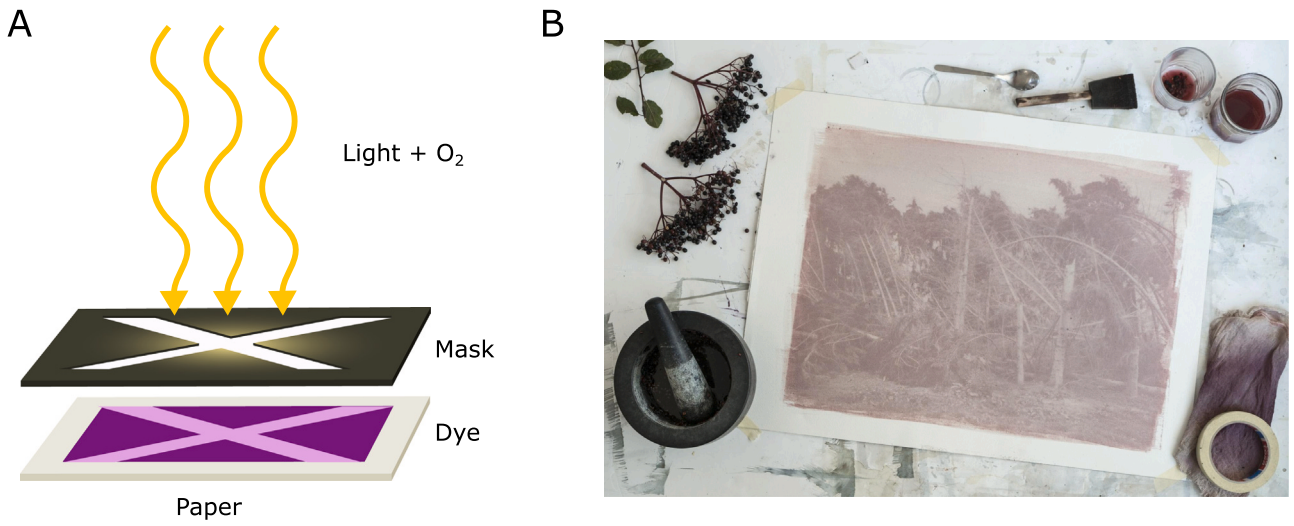

Fig. 1. (A) Schematic setup for anthotype photography – an early method of transferring images from a transparent to a sheet of paper – to selectively bleach a dye in the presence of light and oxygen; (B) example of an anthotype photograph by K. Vrancken based on the photobleaching of anthocyanin dye [54].

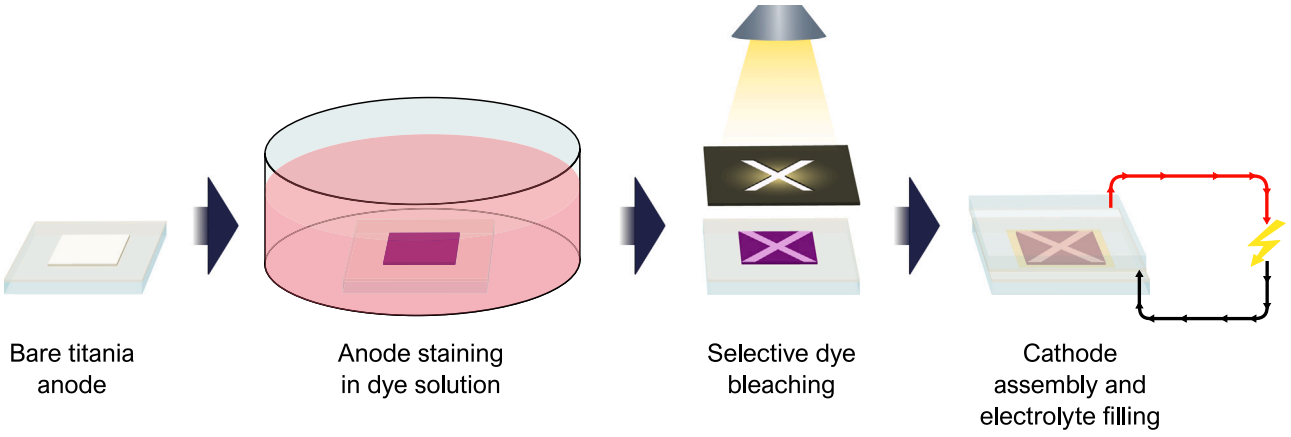

Fig. 2. The production process of photovoltaic photographs: after the procedure of staining of the anode, and before the sealing of the cell, the photoanode is selectively bleached by use of a mask.

photoanodes (Solaronix, Switzerland). In the case of small-scale tests, the FTO (TCO22-7) coated glass plates had an active area of 6×6 mm^2 consisting of a multi-layer TiO_2 architecture of transparent Ti-Nanoxide T/SP covered by a reflective layer of Ti-Nanoxide R/SP. These cells are referred to as the test cells. The anodes of the larger demonstrator cells comprise an active area of 9×9 cm^2 and had the same transparent conducting FTO (TCO22-7) coating with only the Ti-Nanoxide T/SP layer. All anode materials as well as platinized cathodes and electrolyte solution (Iodolyte AN-50) were purchased from Solaronix (Switzerland).

2.4. Dye solution preparation

Anthocyanin pigments were extracted from black rice (Oryza sativa L. indica). The chemical structure of anthocyanins is depicted in Fig. 4. Cyanidin-3-O-glucoside and peonidin-3-O-glucoside are the two major anthocyanins found in black rice [55]. The hydroxyl and methoxy functional groups are known to bind well to the titania surface of the photoanode [40,41,56]. A solution was prepared by soaking 500 g of dry black rice in 500 ml 96% ethanol (Sigma-Aldrich) at 55 °C in a heat bath. After 5 h, the mixture was vacuum-filtered using filter paper type MN 640 m (Macherey-Nagel, Germany). The filtration ensured the removal of undissolved organic material that would otherwise contaminate the device. The dye solution was kept in an airtight bottle and stored in a dark environment at room temperature.

Ruthenizer 535-bisTBA, more commonly known as N719 (Solaronix, Switzerland), was dissolved in a solution of 3×10^{-4} M in 96% ethanol for a couple of hours, resulting in a dark red solution. The solution was stored airtight in a dark environment to prevent degradation. Prior to usage, the quality of the solution was verified by checking for brown discoloration which would indicate oxidation of the pigment [57].

2.5. Cell assembly

Assembly of the test cells was done following the procedure documented in Ref. Martineau et al. [57]. In order to reactivate the photoanodes they were re-fired for 15 min at 450 °C before cooling to 60 °C, at which point the cells were placed in the staining solution. After staining for 6 h, the photoanodes were rinsed with ethanol and dried with pressurized air. The platinized electrodes were also re-fired for 15 min at 450 °C. The cells were assembled using a Meltonix sealing gasket placed between the photoanode and the cathode while applying heat and pressure. The electrolyte was injected through a hole in the platinized electrode, whereupon the cells were sealed by means of Meltonix sealing film and a glass cap. All Meltonix sealing products were obtained from Solaronix (Switzerland). Lastly, silver paste was applied to the electrodes to enhance charge collection and enable a low contact resistance.

2.6. Details on the bleaching procedure

The selective bleaching of the photoanodes took place immediately after staining. Bleaching experiments were performed using a solar simulator: a Xenon arc lamp Model 6690 (Thermo Oriel, USA). Stained anodes were either fully covered (kept in dark), not covered or partly covered. In the case of the latter, masks were made from optically thick sticker material fixed to microscope slides. These masks have an 11.4 mm^2 area cut-out depicting an X at their center. They are placed between the light source and the anodes, with the titania facing away from the light, *i.e.* with the same light path direction as during the operation of a finished solar cell. Anoxygenic experiments were conducted by performing the bleaching step in an airtight chamber filled with N_2 gas during illumination. The windows of these chambers were made of the same type of glass that the masks were made out of. They were (besides atmospheric gas) the only optical obstacle between the light source and the anodes, guaranteeing identical light paths to those in the experiments that were performed in air. The input power of the light source was set to 150 W, resulting in an irradiance of 6 kW/m^2 at the distance of the anodes. The test cells were bleached by exposing them for 18 h in the case for anthocyanin. Due to its superior photostability, N719 required an exposure time of 22 h. A black background was utilized to prevent undesired light scattering. The R3L3S1N negative USAF1951 test chart (Thorlabs, USA) was used as a mask to obtain the resolution of the imaging technique. These resolution tests were captured using a Dino-Lite Digital Microscope Premier AM4113ZT(R4).

2.7. Demonstrator cells

Preparation of the demonstrator cells proceeded in a similar manner, the only notable difference being the larger photoactive area and only containing the Ti-Nanoxide T/SP layer on the anode, resulting in a semi-transparent solar cell. The photoanodes were subsequently stained by soaking in a dye solution bath for at least 20 h. Images were transferred to demonstrator cells by placing transparencies, printed by a common inkjet printer, between the cells and the light source, after which the cells were bleached for 7.5 h (anthocyanin) or 23 h (N719).

2.8. IV measurements

IV measurements were recorded using a Keithley 2602 A source meter. Three devices of each type of test cell were fabricated (fully covered, partly covered and not covered). The full active area of 6×6 mm^2 of the cells was illuminated under an AM1.5G irradiance simulated solar light from a class A solar simulator by Abet Technologies. The light source was calibrated by a reference c-Si solar cell certified by ISE Fraunhofer to guarantee a total incident power of 1000 W/m^2. A voltage sweep was taken from −0.20 V to 0.70 V at 0.01 V intervals. Due to inherent diffusion mechanisms in a dye-sensitized solar cell, prior light soaking up to 1 min was needed to reach a maximum current output [58]. Measurements were performed in a temperature controlled lab at 21 °C.

3. Results and discussion

3.1. Photo-induced patterning on small-scale cells

Two dyes were explored to prepare photovoltaic photographs using DSSC devices: anthocyanins – natural pigments extracted from plants – and a common ruthenium based dye, known as N719. The effects of bleaching the two dyes are studied both by visual inspection and by IV characterization of the finished DSSCs. These experiments were performed on small-scale cells with a photoactive area of 6×6 mm^2 (see the Materials and methods section for details on the fabrication of the devices).

3.1.1. The effect of light and oxygen on pigment bleaching

Fig. 3 depicts photographs of finished cells made using anthocyanin and N719 dyes after exposure to light during the fabrication process. Here we make the distinction between three cases: one set of cells was immediately covered after staining to ensure a dark environment, another set got completely exposed to light, and a third set of cells got partly covered by means of a mask containing an X-imprint (detailed description in the Materials and methods section). The top rows depict the effect of photobleaching in air, while the cells in the bottom rows were placed in a chamber in N_2 atmosphere during exposure. In the presence of O_2, anthocyanins are strongly affected by light; there is a clear visual contrast between areas of photoanode that were exposed to light and areas that were covered. A comparison between the oxygenic and anoxygenic environments demonstrates that O_2 plays a crucial role in the degradation of the dye. As a side remark, we mention that the cell with the X-imprint also shows signs of bleaching on the areas covered by the mask, which is likely caused by scattered light.

In the case of N719, the bleaching effect is less pronounced. However, the cells yield a significantly higher photovoltaic output than for the case of the anthocyanin dye. Either this pigment is more photostable or there is no strong contrast in color intensity between the pigment and its photobleached counterpart. Still, it remains possible to transfer an image with this technique. The anodes that were kept anoxygenic during the light exposure show no visual signs of bleaching. Furthermore, there is a striking contrast between the covered anodes with and without O_2, suggesting that O_2 affects the pigment and that bleaching occurs even though the cell is not illuminated.

From the analysis of these photo-patterned solar cells, it is clear that the combination of light and O_2 drives the bleaching mechanism. This finding provides tentative evidence for the production of reactive oxygen species (ROS) during the bleaching process, as it is a known mechanism for photobleaching in anthocyanins [59]. Yet, in the case without O_2 presence, slight bleaching is also observed in the partly covered cell as a faint imprint of the X. This might hint towards a supplementary pathway of anoxygenic bleaching. However, residual O_2 or leakage of the sample chamber could equally well explain this effect. Further work should elucidate the exact nature of this bleaching mechanism.

It is known that the principle of anthotype photography is based on the mechanism of oxygenic photobleaching. Photo-induced degradation of several organic dyes, *e.g.* anthocyanins [59,60] can occur due to reactive oxygen species (ROS) that are photosensitized in the presence of light and O_2. The presence of molecular oxygen reacting with excited fluorophores can generate ROS, of which the production of singlet oxygen ($^1O_2$*) is the most important in many cases, reacting rapidly with the exposed chemical groups in organic dyes [61]. Fig. 4 presents the tentative mechanism behind ROS photosensitization: when the photosensitizer dye is excited to the S_1 state and when it exhibits intersystem crossing to the T_1 state, it can either decay by phosphorescence emission or transfer the excitation energy to the ground-state triplet oxygen ($^3O_2$) to result in the formation of $^1O_2$*. This species can emit phosphorescence in the near-IR region, but being highly reactive, it is able to activate different photochemical processes, including the irreversible photo-oxidation of the dye [60].

In the case of DSSCs, a different mechanism is generally proposed for the production of ROS. When dye molecules, adsorbed on the surface of TiO_2 nanoparticles, absorb light energy, they can inject electrons into the conduction band of TiO_2. This excitation triggers the photocatalytic process by which adsorbed O_2 is converted to the superoxide radical O_2^- [62]. This species is scavenged by anthocyanin molecules, resulting in photo-oxidative degradation of the dye. There exist other intricate pathways by which the photocatalytic process generates ROS, which are discussed in detail elsewhere [62,63].

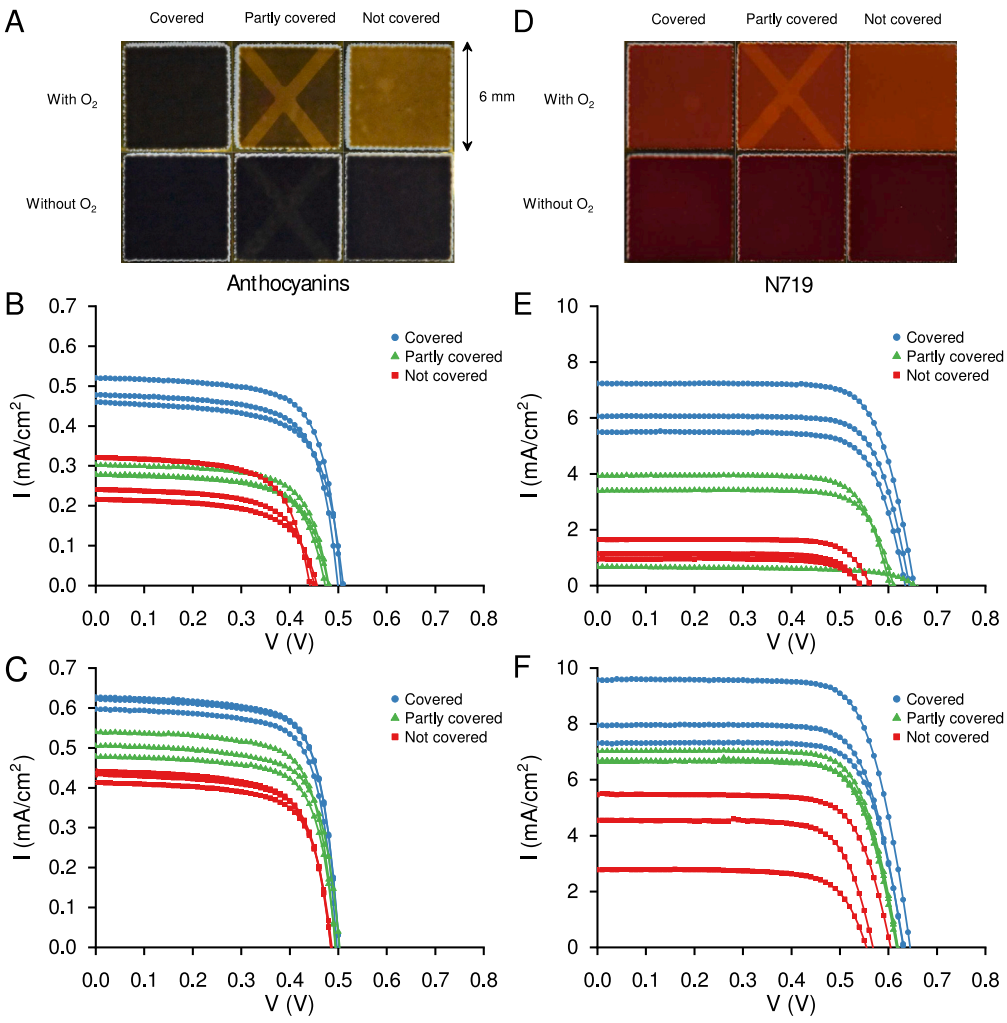

Fig. 3. Photographs of finished cells made from (A) anthocyanins and (D) N719 at different storage conditions after staining illustrate the importance of O_2 and light in the bleaching process. IV curves show a drop in performance as the bleached area increases for: (B) anthocyanin in O_2 atmosphere, (C) anthocyanin in N_2 atmosphere, (E) N719 in O_2 atmosphere and (F) N719 in N_2 atmosphere.

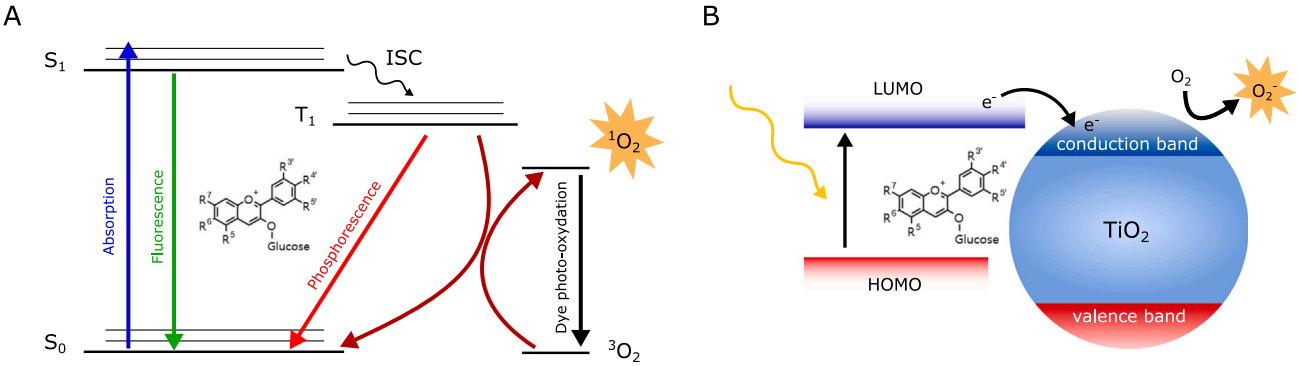

Fig. 4. (A) The generation of singlet oxygen $^1O_2$* by the photosensitization of anthocyanins in anthotype photography. (B) The mechanism behind ROS generation by the photocatalytic process in dye-stained TiO_2 nanoparticles.

3.1.2. The effect of light and oxygen during fabrication on photovoltaic performance

The IV curves are depicted in Fig. 3 for anthocyanin in air (B), anthocyanin in N_2 (C), N719 in air (E) and N719 in N_2 (F). Table 1 lists the average IV characteristics: short-circuit current J_{sc}, open-circuit voltage V_{oc}, fill factor FF, and efficiency η. Three cells were prepared for each variant. Although this is insufficient for adequate statistical analysis, we still can see the overall adverse effect of bleaching emerging in the IV characteristics. In all cases a drop in performance is observed going from the covered to the not covered anodes. Focusing on the tests performed in air, there is a confirmation of the visual analysis as we notice a decrease in performance with increasing area of bleached photoanode, especially considering J_{sc} and η. This is to be expected, since bleached pigments lose their ability to absorb light and therefore cannot transfer any photoelectrons to the TiO_2. Nonetheless,

Table 1
IV Characteristics obtained for variants of DSSCs. Each result is the average of three test cells, with the standard error on the last digit displayed between brackets.

Samples	J_{sc} [mA/cm^2]	V_{oc} [V]	FF	η [%]
Not sensitized	0.12	0.38	0.51	0.02
Anthocyanin in air, covered	0.49(3)	0.506(6)	0.69(1)	0.17(2)
Anthocyanin in N_2, covered	0.62(2)	0.500(2)	0.727(3)	0.224(8)
Anthocyanin in air, partly covered	0.29(2)	0.478(4)	0.669(7)	0.091(6)
Anthocyanin in N_2, partly covered	0.51(3)	0.497(5)	0.714(4)	0.18(1)
Anthocyanin in air, not covered	0.26(6)	0.449(8)	0.64(2)	0.08(2)
Anthocyanin in N_2, not covered	0.43(2)	0.486(1)	0.694(3)	0.145(4)
N719 in air, covered	6.3(9)	0.64(1)	0.757(5)	3.1(5)
N719 in N_2, covered	8(1)	0.636(8)	0.749(8)	3.9(6)
N719 in air, partly covered[a]	3.7(4)	0.607(6)	0.767(6)	1.7(2)
N719 in N_2, partly covered	6.8(2)	0.619(2)	0.751(4)	3.15(9)
N719 in air, not covered	1.2(4)	0.55(1)	0.75(1)	0.5(2)
N719 in N_2, not covered	4(1)	0.58(3)	0.737(8)	1.8(7)

[a]Due to a defective device the results of only two test samples were averaged to obtain these values.

the partially bleached cells depicting an X still generate a significant current. Likewise, a smaller, but significant drop in V_{oc} is measured for both dyes each time the proportion of exposed area increases. The exact nature of this voltage drop is unknown at the moment. Likely this originates from the loss of light absorption, hereby decreasing the photo-generation current which causes a drop in voltage [64]. We also observe that fully bleached cells perform better than cells that were not sensitized, indicating that either some dye molecules stay intact after bleaching or that the photodegraded reaction products retain some photosensitizing functionality.

For best contrast of the X-imprint, the anodes should be exposed to air during bleaching. Not surprisingly, these cells show a drop in efficiency (46(7)% for anthocyanin and 45(11)% for N719) compared to the covered cells. It should be noted that the loss in performance depends on the image imprinted on the anode. A lighter image with large bleached areas will for instance yield a lower photovoltaic output than darker images, *i.e.* less bleached. This corresponds with the earlier mentioned general drawback of patterned solar cells, *i.e.* the intrinsic trade-off between efficiency and transparency. An important finding is that once the cells are isolated from O_2, the bleaching mechanism is inhibited. This means that photobleaching of the pigments can be suppressed by encapsulation, such that a finished cell can be exposed to light without significant degradation. This creates a pathway for novel applications such as the implementation of an intrinsic image into a fully functional and stable DSSC.

3.2. Photo-induced bleaching allows images with high contrast and resolution

Following the proof-of-principle of our technique to transfer an image onto a DSSC, one might ask what spatial resolution can be reached. In the case of anthocyanin, the observation of cells bleached under the USAF-1951 resolution test chart in Fig. 5 reveals a resolution of 45.3 lp/mm (lp: linepairs), corresponding to a minimum linewidth of 11.05 μm. Considering N719, we observe that the contrast between the bleached and the not-bleached areas is not as pronounced as for anthocyanin. The resolution is quantified by means of the acutance, which can be determined by the edge-spread-function [65]. This technique revealed a 10%–90% rise distance of 20.0(5) μm for anthocyanin and 21.3(11) μm for N719 (See Fig. 5 (C)), meaning there is no significant difference in acutance between both dyes. These values demonstrate the potential of our technique compared to inkjet-printed DSSCs, which are restricted to a drop spacing of 30 μm [30]. Limits in the resolution of our bleaching technique might have several origins, including: mask definition, light source collimation, light diffraction, light scattering and ROS diffusion.

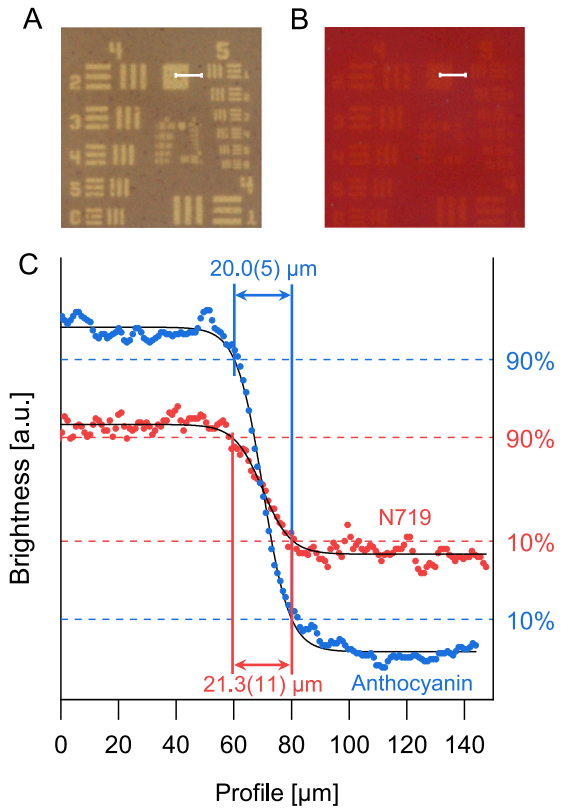

Fig. 5. Prints of the USAF-1951 resolution test chart were transferred to photoanodes stained with (A) anthocyanin and (B) N719. An intensity profile (C) was taken along the white bars which reveals a similar 10%-90% rise distance of both dyes of ~ 20μm.

3.3. Photo-induced bleaching is a scalable technique

To demonstrate the full potential of this new technique, a large-scale prototype was devised with an active area of 9 × 9 cm^2. The finished solar cell is depicted in Fig. 6 and shows a semi-transparent DSSC imprinted with an image of the portrait *Girl with a Pearl Earring* by Johannes Vermeer (1632–1675). For comparison, we fabricated a similar solar cell using N719 as photosensitizer (see Fig. 6). This cell performs better, but has a lower image quality compared to the anthocyanin stained DSSC due to inferior contrast properties. Notably, the fabrication of large-scale photovoltaic photographs takes as long as that of the small-scale cells, demonstrating the size-independent nature of this technique and promising a fast transition to large-area application in BIPV.

4. Conclusions

This work is the first step in the development of photovoltaic photographs containing a patterned 2D-photoactive layer by using a direct photo-induced patterning process, *i.e.* one-step photolithography in the presence of oxygen to induce selective photobleaching in the photoactive layer. As a proof-of-principle for the concept of photovoltaic photographs, demonstrators (up to 9 × 9 cm^2) have been realized using dye-sensitized solar cells, due to ease of fabrication and broad variety of available colors. We found that DSSCs can be selectively bleached by strong illumination in the presence of O_2 and that an image can be fixated after encapsulation. This patterning technique can be integrated in the existing production process without modification of the staining and assembly procedures. A proof-of-principle using anthocyanins extracted from renewable sources, in this case black rice, provided high-contrast, high-resolution images. As is the case for any patterning technique, a loss in performance is an inevitable downside, but losses can be mitigated by appropriate choice of images to portray.

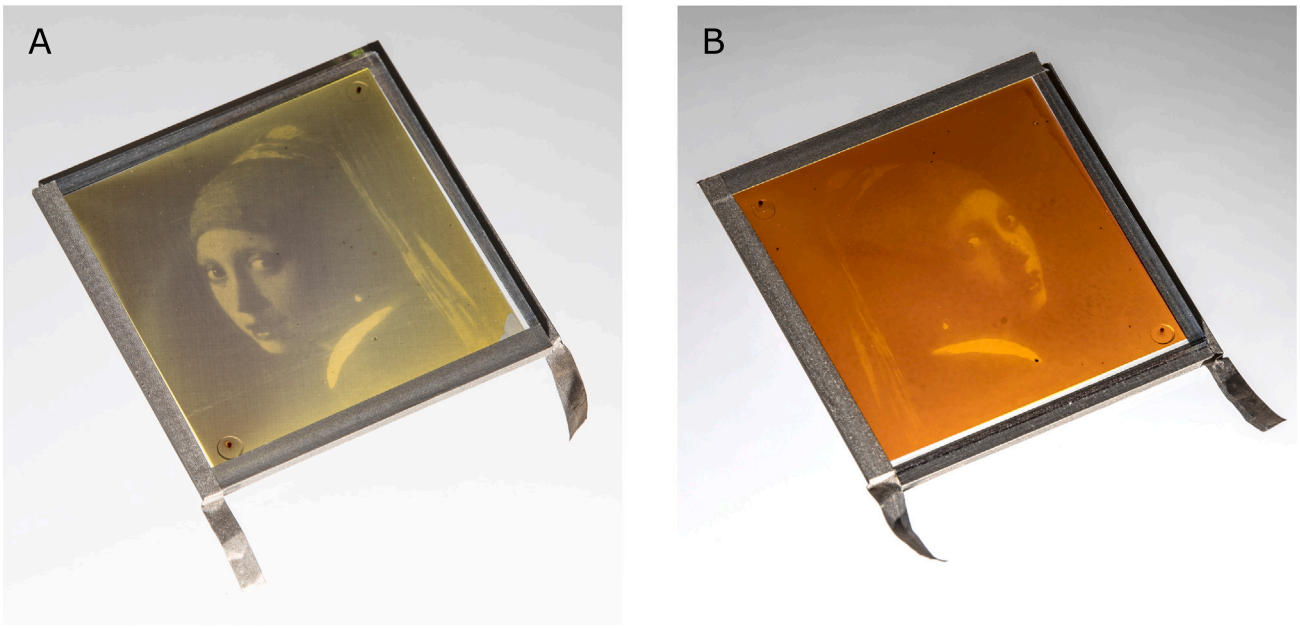

Fig. 6. A 9×9 cm^2 photovoltaic photograph displaying the portrait of *Girl with a Pearl Earring* by Johannes Vermeer, realized by selectively bleaching the anthocyanin (left) and the N719 (right) stained anode.

We also proved that our technique is suitable for the high-performance, synthetic dye N719. The images obtained with this dye have a lower contrast, but they exhibit a similar resolution.

The presented technique offers increased aesthetical and design freedom possibilities in PV technology. The image is integrated directly into the photoactive layer, whereas other approaches might require the additional application of an external layer which is sensitive to weathering. The fabrication procedure is easy to implement in existing production lines since the patterning process is compatible with traditional production steps and requires no big investments, resulting in the inexpensive nature of the process. Furthermore, the preparation time is independent of size, allowing for fast upscaling to large-area devices. The high-resolution patterning process ensures high quality of the images, and although the transferred images are monochromatic, they are available in varying grayscale. The universality of the bleaching step creates the potential of this methodology to be transferred to other classes of emerging solar cells.

Further work should focus on unraveling the details of the underlying photo-induced bleaching mechanism in the photoactive film, with the goal of an improved understanding and more control of the technique. Considering PV performance, of further relevance will be the study of the occurrence and impact of induced electronic defects and the trade-off between absorption, semi-transparency and photovoltaic output. Additionally, long-term stability in operational conditions needs to be studied, to monitor the resilience of performance and appearance against long-duration exposure to sunlight.

The devices reported here introduce the concept of photovoltaic photographs and have to be considered as the exploratory starting point. With the presented concept and insights we aim to inspire further exploration in combining these processes with other PV technologies (*e.g.* organic and perovskite solar cells) to enhance the aesthetical and design possibilities of solar cells.

CRediT authorship contribution statement

Jeroen Hustings: Data curation, Formal analysis, Investigation, Methodology, Visualization, Writing – original draft. **Nico Fransaert:** Data curation, Formal analysis, Investigation, Methodology, Writing – original draft. **Kristof Vrancken:** Resources, Writing – review & editing. **Rob Cornelissen:** Writing – review & editing. **Roland Valcke:** Writing – review & editing. **Jean V. Manca:** Conceptualization, Funding acquisition, Project administration, Supervision, Writing – original draft.

Declaration of competing interest

The authors declare that they have no known competing financial interests or personal relationships that could have appeared to influence the work reported in this paper.

Data availability

Data will be made available on request.

Acknowledgments

The authors thank the colleagues from X-LAB from UHasselt for discussions and feedback. Special thanks to M. De Roeve for help with the experimental setup. This research was supported by the Research Foundation – Flanders (FWO) with research project G089918N (J.H. and J.M.) and PhD Fellowship with application number 11K4322N (N.F.).

References

[1] S. Yoon, S. Tak, J. Kim, Y. Jun, K. Kang, J. Park, Application of transparent dye-sensitized solar cells to building integrated photovoltaic systems, Build. Environ. 46 (10) (2011) 1899–1904.
[2] J. Sun, J.J. Jasieniak, Semi-transparent solar cells, J. Phys. D: Appl. Phys. 50 (9) (2017) 093001.
[3] D.H. Shin, S.-H. Choi, Recent studies of semitransparent solar cells, Coatings 8 (10) (2018) 329.
[4] P. Selvaraj, A. Ghosh, T.K. Mallick, S. Sundaram, Investigation of semi-transparent dye-sensitized solar cells for fenestration integration, Renew. Energy 141 (2019) 516–525.
[5] K.-S. Chen, J.-F. Salinas, H.-L. Yip, L. Huo, J. Hou, A.K.Y. Jen, Semi-transparent polymer solar cells with 6% PCE, 25% average visible transmittance and a color rendering index close to 100 for power generating window applications, Energy Environ. Sci. 5 (2012) 9551–9557.
[6] B. Shi, L. Duan, Y. Zhao, J. Luo, X. Zhang, Semitransparent perovskite solar cells: From materials and devices to applications, Adv. Mater. 32 (3) (2020) 1806474.
[7] S.Y. Myong, S.W. Jeon, Design of esthetic color for thin-film silicon semi-transparent photovoltaic modules, Sol. Energy Mater. Sol. Cells 143 (2015) 442–449.

[8] S. Aharon, M. Layani, B.-E. Cohen, E. Shukrun, S. Magdassi, L. Etgar, Solar cells: Self-assembly of perovskite for fabrication of semitransparent perovskite solar cells (Adv. Mater. Interfaces 12/2015), Adv. Mater. Interfaces 2 (2015) 5584.

[9] G.E. Eperon, V.M. BURL:akov, A. Goriely, H.J. Snaith, Neutral color semi-transparent microstructured perovskite solar cells, ACS Nano 8 1 (2014) 591–8–8.

[10] Q. Tai, F. Yan, Emerging semitransparent solar cells: Materials and device design, Adv. Mater. 29 (34) (2017) 1700192.

[11] S. Shafian, J. Son, Y. Kim, J.K. Hyun, K. Kim, Active-material-independent color-tunable semitransparent organic solar cells, ACS Appl. Mater. Interfaces 11 (21) (2019) 18887–18895.

[12] K.-T. Lee, L.J. Guo, H.J. Park, Neutral- and multi-colored semitransparent perovskite solar cells, Molecules 21 (4) (2016) 475.

[13] N. Robertson, Optimizing dyes for dye-sensitized solar cells, Angew. Chem. Int. Ed. 45 (15) (2006) 2338–2345.

[14] A.J. Nozik, Quantum dot solar cells, Physica E 14 (1) (2002) 115–120.

[15] S. Rühle, M. Shalom, A. Zaban, Quantum-dot-sensitized solar cells, ChemPhysChem 11 (11) (2010) 2290–2304.

[16] X. Li, Z. Ku, Y. Rong, G. Liu, L. Liu, T. Liu, M. Hu, Y. Yang, H. Wang, M. Xu, P. Xiang, H. Han, Design of an organic redox mediator and optimization of an organic counter electrode for efficient transparent bifacial dye-sensitized solar cells, Phys. Chem. Chem. Phys. 14 (2012) 14383–14390.

[17] G. Li, C.W. Chu, V. Shrotriya, J. Huang, Y. Yang, Efficient inverted polymer solar cells, Appl. Phys. Lett. 88 (25) (2006) 253503.

[18] X.-L. Ou, M. Xu, J. Feng, H.-B. Sun, Flexible and efficient ITO-free semi-transparent perovskite solar cells, Sol. Energy Mater. Sol. Cells 157 (2016) 660–665.

[19] H. Schmidt, H. Flügge, T. Winkler, T. Bülow, T. Riedl, W. Kowalsky, Efficient semitransparent inverted organic solar cells with indium tin oxide top electrode, Appl. Phys. Lett. 94 (24) (2009) 243302.

[20] C. Xu, P. Shin, L. Cao, J. Wu, D. Gao, Ordered TiO_2 nanotube arrays on transparent conductive oxide for dye-sensitized solar cells, Chem. Mater. 22 (2010) 143.

[21] S.K. Hau, H.-L. Yip, J. Zou, A.K.Y. Jen, Indium tin oxide-free semi-transparent inverted polymer solar cells using conducting polymer as both bottom and top electrodes, Org. Electron. 10 (7) (2009) 1401–1407.

[22] K. Sun, P. Li, Y. Xia, J. Chang, J. Ouyang, Transparent conductive oxide-free perovskite solar cells with PEDOT:Pss as transparent electrode, ACS Appl. Mater. Interfaces 7 (28) (2015) 15314–15320.

[23] Z. Zhang, R. Lv, Y. Jia, X. Gan, H. Zhu, F. Kang, All-carbon electrodes for flexible solar cells, Appl. Sci. 8 (2) (2018) 152.

[24] Z. Liu, P. You, S. Liu, F. Yan, Neutral-color semitransparent organic solar cells with all-graphene electrodes, ACS Nano 9 (12) (2015) 12026–12034.

[25] H. Wang, H. Liu, W. Li, L. Zhu, H. Chen, Inorganic perovskite solar cells based on carbon electrodes, Nano Energy 77 (2020) 105160.

[26] Z. Huang, X. Liu, K. Li, D. Li, Y. Luo, H. Li, W. Song, L. Chen, Q. Meng, Application of carbon materials as counter electrodes of dye-sensitized solar cells, Electrochem. Commun. 9 (4) (2007) 596–598.

[27] T.E. Kuhn, C. Erban, M. Heinrich, J. Eisenlohr, F. Ensslen, D.H. Neuhaus, Review of technological design options for building integrated photovoltaics (BIPV), Energy Build. 231 (2021) 110381.

[28] Kameleonsolar, portfolio, 2021, URL: https://kameleonsolar.com/portfolio/.

[29] M. Mittag, M. Ebert, H.R. Wilson, T. Fellmeth, Mosaic module concept for cost-efficient and aesthetic BIPV modules, in: 35th European Photovoltaic Solar Energy Conference and Exhibition; Vol. 1458-1462, 2018, pp. 1458–1462.

[30] S.G. Hashmi, M. Ozkan, J. Halme, S.M. Zakeeruddin, J. Paltakari, M. Gratzel, P.D. Lund, Dye-sensitized solar cells with inkjet-printed dyes, Energy Environ. Sci. 9 (7) (2016) 2453–2462.

[31] S.G. Hashmi, D. Martineau, X. Li, M. Ozkan, A. Tiihonen, M.I. Dar, T. Sarikka, S.M. Zakeeruddin, J. Paltakari, P.D. Lund, M. Grätzel, Air processed inkjet infiltrated carbon based printed Perovskite solar cells with high stability and reproducibility, Adv. Mater. Technol. 2 (1) (2017) 1600183.

[32] J. Zhao, N. Chai, X. Chen, Y. Yue, Y.-B. Cheng, J. Qiu, X. Wang, Nonthermal laser ablation of high-efficiency semitransparent and aesthetic perovskite solar cells, Nanophotonics 11 (5) (2022) 987–993.

[33] M.A. Green, E.D. Dunlop, J. Hohl-Ebinger, M. Yoshita, N. Kopidakis, X. Hao, Solar cell efficiency tables (version 59), Prog. Photovolt., Res. Appl. 30 (1) (2022) 3–12.

[34] A. Fakharuddin, R. Jose, T.M. Brown, F. Fabregat-Santiago, J. Bisquert, A perspective on the production of dye-sensitized solar modules, Energy Environ. Sci. 7 (12) (2014) 3952–3981.

[35] N. Kumara, A. Lim, C.M. Lim, M.I. Petra, P. Ekanayake, Recent progress and utilization of natural pigments in dye sensitized solar cells: A review, Renew. Sustain. Energy Rev. 78 (2017) 301–317.

[36] L. Yang, J. Feng, Z. Liu, Y. Duan, S. Zhan, S. Yang, K. He, Y. Li, Y. Zhou, N. Yuan, J. Ding, S. Liu, Record-efficiency flexible perovskite solar cells enabled by multifunctional organic ions interface passivation, Adv. Mater. 34 (24) (2022) 2201681.

[37] F. De Rossi, G. Renno, B. Taheri, N. Yaghoobi Nia, V. Ilieva, A. Fin, A. Di Carlo, M. Bonomo, C. Barolo, F. Brunetti, Modified P3HT materials as hole transport layers for flexible perovskite solar cells, J. Power Sources 494 (2021) 229735.

[38] H.M. Lee, J.H. Yoon, Power performance analysis of a transparent DSSC BIPV window based on 2 year measurement data in a full-scale mock-up, Appl. Energy 225 (2018) 1013–1021.

[39] G. Calogero, G. Di Marco, S. Caramori, S. Cazzanti, R. Argazzi, C.A. Bignozzi, Natural dye senstizers for photoelectrochemical cells, Energy Environ. Sci. 2 (11) (2009) 1162–1172.

[40] S. Shalini, R.B. Prabhu, S. Prasanna, T.K. Mallick, S. Senthilarasu, Review on natural dye sensitized solar cells: Operation, materials and methods, Renew. Sustain. Energy Rev. 51 (2015) 1306–1325.

[41] N.A. Ludin, A. Mahmoud, A.B. Mohamad, A.A.H. Kadhum, K. Sopian, N.S.A. Karim, Review on the development of natural dye photosensitizer for dye-sensitized solar cells, Renew. Sustain. Energy Rev. 31 (2014) 386–396.

[42] M. Kokkonen, P. Talebi, J. Zhou, S. Asgari, S.A. Soomro, F. Elsehrawy, J. Halme, S. Ahmad, A. Hagfeldt, S.G. Hashmi, Advanced research trends in dye-sensitized solar cells, J. Mater. Chem. A 9 (17) (2021) 10527–10545.

[43] E. Barraud, Stained glass solar windows for the Swiss tech convention center, CHIMIA 67 (3) (2013) 181.

[44] H. Yuan, W. Wang, D. Xu, Q. Xu, J. Xie, X. Chen, T. Zhang, C. Xiong, Y. He, Y. Zhang, Y. Liu, H. Shen, Outdoor testing and ageing of dye-sensitized solar cells for building integrated photovoltaics, Sol. Energy 165 (2018) 233–239.

[45] M.H. Chung, B.R. Park, E.J. Choi, Y.J. Choi, C. Lee, J. Hong, H.U. Cho, J.H. Cho, J.W. Moon, Performance level criteria for semi-transparent photovoltaic windows based on dye-sensitized solar cells, Sol. Energy Mater. Sol. Cells 217 (2020) 110683.

[46] M. Szindler, M. Szindler, A. Drygała, K. Lukaszkowicz, P. Kaim, R. Pietruszka, Dye-sensitized solar cell for building-integrated photovoltaic (BIPV) applications, Materials 14 (13) (2021) 3743.

[47] M.-E. Yeoh, K.-Y. Chan, A review on semitransparent solar cells for real-life applications based on dye-sensitized technology, IEEE J. Photovolt. 11 (2) (2021) 354–361.

[48] L.E. Garner, V. Nellissery Viswanathan, D.H. Arias, C.P. Brook, S.T. Christensen, A.J. Ferguson, N. Kopidakis, B.W. Larson, Z.R. Owczarczyk, J.R. Pfeilsticker, P.C. Ramamurthy, S.H. Strauss, O.V. Boltalina, W.A. Braunecker, Photobleaching dynamics in small molecule vs. polymer organic photovoltaic blends with 1,7-bis-trifluoromethylfullerene, J. Mater. Chem. A 6 (11) (2018) 4623–4628.

[49] B. Liu, Y. Han, Z. Li, H. Gu, L. Yan, Y. Lin, Q. Luo, S. Yang, C.-Q. Ma, Visible light–Induced degradation of inverted polymer:Nonfullerene acceptor solar cells: Initiated by the light absorption of ZnO layer, Solar RRL 5 (1) (2021) 2000638.

[50] N.H. Nickel, F. Lang, V.V. Brus, O. Shargaieva, J. Rappich, Unraveling the light-induced degradation mechanisms of $CH_3NH_3PbI_3$ perovskite films, Adv. Electron. Mater. 3 (12) (2017) 1700158.

[51] J. Herschel, On the Action of the Rays of the Solar Spectrum on Vegetable Colours, and on Some New Photographic Processes, Taylor, 1842, URL: https://books.google.be/books?id=Ic91ZbyHSYEC.

[52] H.H. Snelling, The History and Practice of the Art of Photography, G. P. PUTNAM, 155 Broadway, New York, US, 1849.

[53] N. Perkič, M. Gorjanc, The influence of after-treatments on dyeability of raw and bleached cotton with curcumin, and visibility of anthotype produced motifs, TEKSTILEC 60 (1) (2017) 4–13.

[54] K. Vrancken, The Sustainist Gaze, (Ph.D. thesis), LUCA School of Arts, 2022, URL: https://sustainistgaze.com/.

[55] C. Hu, J. Zawistowski, W. Ling, D.D. Kitts, Black rice (oryza satival.indica) pigmented fraction suppresses both reactive oxygen species and nitric oxide in chemical and biological model systems, J. Agricult. Food Chem. 51 (18) (2003) 5271–5277.

[56] M.H. Buraidah, L.P. Teo, S.N.F. Yusuf, M.M. Noor, M.Z. Kufian, M.A. Careem, S.R. Majid, R.M. Taha, A.K. Arof, TiO2/Chitosan-NH4I(+I-2)-BMII-Based dye-sensitized solar cells with anthocyanin dyes extracted from black rice and red cabbage, Int. J. Photoenergy (2011) 11.

[57] D. Martineau, Dye solar cells for real, Report, Solaronix, 2012.

[58] G. Bardizza, D. Pavanello, R. Galleano, T. Sample, H. Mullejans, Calibration procedure for solar cells exhibiting slow response and application to a dye-sensitized photovoltaic device, Sol. Energy Mater. Sol. Cells 160 (2017) 418–424.

[59] H. Yamasaki, H. Uefuji, Y. Sakihama, Bleaching of the red anthocyanin induced by superoxide radical, Arch. Biochem. Biophys. 332 (1) (1996) 183–186.

[60] A.P. Demchenko, Photobleaching of organic fluorophores: quantitative characterization, mechanisms, protection, Methods Appl. Fluoresc. 8 (2) (2020) 022001.

[61] M.C. DeRosa, R.J. Crutchley, Photosensitized singlet oxygen and its applications, Coord. Chem. Rev. 233 (2002) 351–371.

[62] A.R. Khataee, M.B. Kasiri, Photocatalytic degradation of organic dyes in the presence of nanostructured titanium dioxide: Influence of the chemical structure of dyes, J. Mol. Catal. A: Chem. 328 (1–2) (2010) 8–26.

[63] P. N, B. R, A.S. Kristoffersen, B. G, P. S, S. K, K. M.D, S.R. Erga, D. Velauthapillai, Enhanced photostability of anthocyanin dye for increased efficiency in natural dye sensitized solar cells, Optik 227 (2021) 166053.

[64] A.M. Hurnada, M. Hojabri, S. Mekhilef, H.M. Hamada, Solar cell parameters extraction based on single and double-diode models: A review, Renew. Sustain. Energy Rev. 56 (2016) 494–509.

[65] S.W. Smith, The Scientist and Engineer's Guide to Digital Signal Processing, California Technical Publishing, P.O. Box 502407, San Diego, CA 92150-2407, 1997, pp. 423–430.